



HAL
open science

Scaling-up of Mesoporous Silica Films via an Eco-efficient UV Processing Method. Part 2: Photoinduced Calcination

Mathilde Sibeaud, C. Croutxé-Barghorn, S. Rigolet, L. Michelin, B. Lebeau,
L. Vidal, A. Chemtob

► To cite this version:

Mathilde Sibeaud, C. Croutxé-Barghorn, S. Rigolet, L. Michelin, B. Lebeau, et al.. Scaling-up of Mesoporous Silica Films via an Eco-efficient UV Processing Method. Part 2: Photoinduced Calcination. *Microporous and Mesoporous Materials*, 2018, 267, pp.235-241. 10.1016/j.micromeso.2018.03.029 . hal-02434807

HAL Id: hal-02434807

<https://hal.science/hal-02434807>

Submitted on 10 Jan 2020

HAL is a multi-disciplinary open access archive for the deposit and dissemination of scientific research documents, whether they are published or not. The documents may come from teaching and research institutions in France or abroad, or from public or private research centers.

L'archive ouverte pluridisciplinaire **HAL**, est destinée au dépôt et à la diffusion de documents scientifiques de niveau recherche, publiés ou non, émanant des établissements d'enseignement et de recherche français ou étrangers, des laboratoires publics ou privés.

Scaling-up of Mesoporous Silica Films via an Eco-efficient UV

Processing Method.

Part 2: Photoinduced Calcination

Mathilde Sibeaud,^{a,b,c} C. Croutxé-Barghorn,^{b,c} S. Rigolet,^{a,c} L. Michelin,^{a,c} B. Lebeau,^{a,c} L. Vidal,^{a,c} A. Chemtob^{a,c}

^a Université de Haute-Alsace, CNRS, IS2M UMR7361, F-68100 Mulhouse, France

^b Université de Haute-Alsace, LPIM EA4567, F-68100 Mulhouse, France

^c Université de Strasbourg, France

Abstract

We describe a fast photocalcination process to prepare highly ordered silica mesoporous films through the use of a low-pressure amalgam arc (λ : 185 / 254 nm). Because radiant power is 2-3 times higher than conventional low-pressure UV lamps, the elimination of the PEO-*b*-PPO-*b*-PEO copolymer template in the 2D hexagonal hybrid film has been completed within 50 min, without damage to the mesostructure. The degradation kinetics are impacted by film thickness and irradiance, but hardly copolymer concentration. Compared to thermocalcination, a narrower pore size distribution and lower energy consumption have been found. Photodegradation mostly originates from a photoablation mechanism induced by radiation at 185 nm, while oxidation due to photogenerated reactive oxygen species plays a minor role. Photocalcination has been combined with an initial photoinduced mesostructuration (detailed in Part 1: Microporous Mesoporous Mater., 257 (2017) 42-50), resulting in an unprecedented “all UV” method to mesoporous silica films. The final process relies on dual wavelength photoactivation: UV_B to form the hybrid copolymer/silica network, a flash intermediate thermal consolidation, and UV_C to decompose the copolymer chains.

Keywords: silica, ultraviolet radiation, mesoporous film, sol-gel, calcination

1. Introduction

In recent years, inorganic and hybrid ordered mesoporous materials have been the focus of extensive studies through their broad scope of applications [1-3]. Thanks to both mesopores and functionalized pore surface, mesoporous materials in the form of films have been applied in various fields, including catalysis, separation, electronic and optical devices [4]. To fully tap their potential of delivering valuable products in the near future, further efforts are nevertheless necessitated in terms of easing scalability, processability, handling and storage of sol-gel precursors [5]. In this respect, we have recently proposed an eco-efficient Light Induced Self-Assembly (LISA) pathway to mesostructured copolymer/silica films, proceeding in the order of minutes, and using photolent

sol-gel precursors formulation reacted in a compact UV irradiation chamber [6]. However, much of the interest of a surfactant-templated synthesis is to ultimately obtain a mesoporous network surrounded by a self-standing silica or organosilica framework [2]. To achieve this, a subsequent removal of the templating agent, as complete as possible, is necessary. High temperature calcination, also referred to as *thermocalcination*, is currently the most conventional method to get rid of the templating agent [7]. It involves sample heating at sufficiently high temperature to decompose the organic template, typically in the 300 – 500 °C range, while preserving the integrity of the oxide network [8]. Although ubiquitous, this method may be regarded as energy-intensive and slow. Especially, if one considers that the cycle times last between 4 to 8 hours, whereas the synthesis of the hybrid silica/surfactant sample by photopolymerization may be complete in the order of minutes. Depending on the oven type, the consumption can reach up to 1 kW h⁻¹. Alternatively, more energy-saving muffle furnaces can be employed, but they have a much higher cost. Additionally, heat is not a selective stimulus, making the preparation of mesoporous ordered organosilica challenging [9, 10]. Therefore, in most applications where a hybrid mesostructure is needed, grafting of organic moieties is performed by post-functionalization of preformed mesoporous inorganic materials [2]. In the case of films, other issues include loss of mechanical integrity due to network distortions and residual constraints arising during calcination. Finally, high temperatures exclude the use of thermally-sensitive surfaces such as plastic substrates [11, 12]. Solvent extraction is the second most widespread method for surfactant removal [13]; it relies on appropriate solvents in which the surfactant is soluble or has good affinities [14, 15]. However, this strategy involves a high amount of mostly organic solvent and can pollute the sample by swelling the silica network. Its efficiency is highly dependent on surfactant structure and may be hindered when the hydrophilic portion of the surfactant molecule is intimately embedded into the silica network [14]. Typically 10 to 80 % of surfactant can be removed after 6 to 24 h [15].

To overcome these limitations, other methodologies have been introduced, among them, the oxidation of the surfactant template using ozone [16] or hydrogen peroxide [17]. Even more

promising is *photocalcination* because of its potential to improve processing conditions and efficiency [18]. Introduced for the first time in 2000, surfactant template photocalcination relies either on low-pressure Hg arcs [18] or excimer lamps [19], both emitting in the UV_C range (100 - 280 nm). Limited radiation penetration of short-wavelengths has focused interests on thin films (thickness < 1 μm). Very few studies have been reported in the literature, which are detailed in **Table 1**. All of them are affected by slow decomposition rates in the order of hours, incomplete characterization of the photocalcined sample in particular as regards to specific surface area, and there is no systematic comparison with thermocalcination in terms of structure, but also energetic performances and environmental impact. In general, photochemical degradation was attributed to a *photochemical effect* [18, 20] — electronic excitation resulting in direct chemical bond dissociation— and/or *photooxidation effect* [21-23] driven by photogenerated reactive oxygen species (ROS), such as ozone, through well-established photochemical reactions [24].

We report herein a new photocalcination process intended to provide many improvements compared to the current short-wavelength systems described in the literature [20]. Our method uses for the first time, a low-pressure Hg amalgam arc, emitting two lines at 185 and 254 nm, which represents an inexpensive and readily available commercial radiation source. As a special feature, it provides a radiant power 2-3 times higher than conventional low-pressure Hg arcs. This lamp is already in use for air [25] and surface disinfection [26], as well as water purification [27]. Our original photocalcination process is characterized by the possibility to treat micrometer thick films ($\geq 1 \mu\text{m}$) and its rapidity (30 min in the best conditions). Another advantage is the possibility to treat large surface areas ($\geq 100 \text{ cm}^2$) because this lamp is available in various lengths and shapes, opening avenues for upscaling. Another indirect advantage is to be able to obtain at least grams of mesoporous materials, enabling analyses that have never been performed in the past with photocalcined samples, such as the determination of specific surface areas by N₂ adsorption/desorption isotherms and silica network's degrees of condensation by ²⁹Si Solid-State NMR spectroscopy. These characterizations are very important to shed light onto the photoinduced

degradation process, which has remained so far elusive in the literature. Last but not least, adding this photocalcination to the initial photoinduced mesostructuration process (see ref. [6] for details) leads, for the first time, to an “all UV method” to mesoporous thin films. Clearly, the challenge is to achieve a complete surfactant removal from a mesostructured copolymer/silica film in the shortest possible time, without affecting the mesophase’s integrity.

Our complete irradiation process relies on dual wavelength photoactivation: UV_B (280-320 nm) to form the hybrid mesostructured network, then UV_C (165 / 254 nm) to decompose the structuring agent with a flash intermediate thermal consolidation (150 °C), which has proven to be essential to preserve the mesostructure. Our starting material is a 4 μm-thick photolabile liquid film composed of alkoxysilane precursor (poly(dimethoxysiloxane), PDMOS) and 45 wt% of a Pluronic triblock copolymer (P123) acting as templating agent. In the best possible conditions, only 70 min were necessary to achieve a 2D hexagonal mesoporous silica film with this 3-step method. Several parameters, such as film thickness, irradiance, copolymer content have been investigated to determine the best conditions for surfactant elimination and mesostructure preservation. Investigation of the impact of radiation wavelength (λ: 185 / 254 nm) and atmosphere composition on degradation kinetics shed light into a photocalcination mechanism proceeding mainly through photoablation.

2. Materials and Methods

2.1 Materials

Mesoporous silica films were synthesized on polished silicon wafers (Siltronix) or 10 × 10 cm glass substrate (Brot). Photoacid generator diphenyliodonium hexafluorophosphate ($\Phi_2I^+PF_6^-$) and surfactant Pluronic 123 (P123) were provided by Sigma Aldrich. Poly(dimethoxysiloxane) (PDMOS) is an oligomeric methoxy precursor provided by ABCR with a proportion of Q₀/Q₁/Q₂/Q₃ species: 4.5/26.5/48.5/20.5 % as determined by ²⁹Si liquid-state NMR spectroscopy.

2.2 Preparation of mesoporous silica films through a coupled photoinduced mesostructuration and calcination process

A homogeneous and photolabile solution containing PDMOS (1 g), P123 (0.45 g, otherwise mentioned in the text), $\Phi_2I^+PF_6^-$ (60 mg) and acetone (1 g) was prepared. After deposition on a glass or silicon wafer using a 4 μm bare coater, the films were placed into an environmental chamber (Memmert HCP 108 hygrometric chamber) where temperature (T) and relative humidity (RH) were set to $T = 30\text{ }^\circ\text{C}$ and $\text{RH} = 60\%$. Film irradiation inside the chamber was performed for 30 min through two fluorescent UV bulbs UV 6 (UV236 system, Waldmann, 280 - 380 nm, electrical power: 36 W) ensuring a homogenous irradiance of 3 mW cm^{-2} at film surface. After irradiation, the resultant P123/silica film was dry and optically transparent. Samples were then treated thermally during 8 min at $150\text{ }^\circ\text{C}$ in a Memmert UM400 oven (1.4 kW). Thermocalcination was performed with a Nabertherm Controller P330 (1.2 kW), by heating the samples during 4 h at $300\text{ }^\circ\text{C}$ after a $1\text{ }^\circ\text{C min}^{-1}$ ramp. Alternatively, photocalcination was carried out at ambient conditions under air during periods spanning from 60 min to 180 min. As shown in **Fig. S1** of the Data in Brief article, the setup was composed of two indium-mercury amalgam low-pressure arcs (NIQ 60/35XL, Heraeus Noble light, electrical power: 85 W) fixed on a reflective metal panel, and exhibiting two irradiation lines at 185 and 254 nm. Replacement of the synthetic quartz (Suprasil[®]) envelope by a conventional quartz enabled to have a single emission ray at 254 nm (NNI 60/35XL, Heraeus Noble light, electrical power: 85 W). The lamp generates limited heat (+ $25\text{ }^\circ\text{C}$ temperature increase maximum during a 4 h exposure at a sample-lamp distance of 1.5 cm). The irradiation device was placed under a fume hood to ensure constant air renewal. **Table 2** displays the estimated irradiance at 185 and 254 nm lines depending on the sample-lamp distance (1.5 – 12 cm). The irradiance value at 185 nm diminishes more significantly with the distance because of absorption by atmospheric oxygen. Note that the irradiance at 254 nm wavelength may also be diminished by ozone absorption, but the fact that lamp was enclosed in a fume hood ensures an effective evacuation of ozone. All irradiance values were

measured with a USB4000 radiometer (Ocean Optics), which can detect emitted wavelengths from 177 to 895 nm. Given that the 185 nm line is close to the low detection limit of the radiometer, the measured irradiance at 185 nm is likely to be slightly underestimated.

2.3 Characterization

Film thickness was determined through Beer-Lambert law by relating the FTIR absorbance value at 3320 cm^{-1} with an experimentally measured thickness obtained via an optical profilometer (Altisurf 500) using a calibration curve. Film thickness was adjusted (see section 3.3) by varying the acetone concentration in the formulation. The acquisition of θ - 2θ diffractograms was performed with a X'Pert Pro (PANalytical) diffractometer using Cu K α radiation ($\lambda = 0.15418\text{ nm}$; $0.5^\circ < 2\theta < 10^\circ$; $0.017^\circ\text{ s}^{-1}$). XRD patterns were directly taken on the sample deposited on silicon wafer. FTIR transmission spectra were obtained directly on films deposited on silicon wafer using a Bruker Vertex 70 with a resolution of 4 cm^{-1} and 32 spectra accumulation. All spectra were baseline corrected and integrated under OPUS 7.0 software. Morphology of the thermo- and photo-calcined products was observed by transmission electron microscope TEM (JEOL ARM-200F). N₂ adsorption and desorption isotherms were performed on a Tristar 3000 (Micrometrics). Calcined samples were degassed under vacuum at 150°C during 12 h. Specific surface area was determined by BET method, average pore diameter and distribution were evaluated from desorption branch by BJH method. ²⁹Si MAS NMR spectra were recorded on a Bruker AVANCE II 300WB spectrometer ($B_0 = 7.1\text{ T}$) operating at 59.61 MHz, with 7 mm double resonance MAS probe at a speed of 4 kHz, with a $\pi/6$ pulse duration of 2 μs , a recycle delay of 80 s, and a high-power proton decoupling (DEC) during the acquisition. ²⁹Si chemical shifts were referenced to tetramethylsilane (TMS). Assignment of NMR resonances was performed with Topspin 3.1 software, spectra deconvolutions using the DMFIT 2015 Software [28]. Condensation degrees were calculated using the equation: $CD = \sum \frac{n \times A(Q_n)}{f}$, where $A(Q_n)$ is the integrated area of the different Q_n siloxane species of the ²⁹Si NMR spectrum, and f the functionality of the silicon atom $f = 4$. Energy consumption was measured by a power meter device (EL-EPM02HQ from HQ).

3. Results and Discussion

3.1 Description of the 3-step UV methodology to mesoporous silica film

Our process includes three consecutive steps:

- a) Formation of a mesostructured P123/silica hybrid film (4 μm thickness, 45 wt% P123) through UV_B irradiation ($\lambda_{\text{max}} = 320 \text{ nm}$, $I = 3 \text{ mW cm}^{-2}$, $t = 30 \text{ min}$).
- b) Flash thermal consolidation (150 °C, $t = 8 \text{ min}$).
- c) Copolymer template calcination under UV_C irradiation ($\lambda = 185 / 254 \text{ nm}$, $I = 63 \text{ mW cm}^{-2}$, $t = 60 \text{ min}$).

The XRD patterns of the film after each stage are shown in **Figure 1**. Following the first step, the as-synthesized copolymer/silica film (pattern **a**) showed a series of low intense peaks, which can be indexed as (100), (200) and (210) reflections of a 2D hexagonal mesostructure ($d_{100} = 2d_{200} = \sqrt{7}d_{210}$, lattice parameter is 89 Å). The thermal consolidation caused a significant intensification of the signals (pattern **b**), suggesting a higher ordering of the mesostructure. Finally, the mesostructure seemed to be retained after photocalcination (pattern **c**) although less intense peaks were visible. The peak position and breadth were not changed compared with the as-synthesized material, indicating similarity as regards siloxane network condensation and mesostructure. More intense XRD peaks were obtained when photocalcination was substituted by thermocalcination (pattern **c'**, 300 °C, $t = 4 \text{ h}$). Comparison between the two calcination methods has been commented in the next section. **Figure 2** depicts the evolution of the CH stretching modes of P123 (2810 - 3020 cm^{-1}) throughout photocalcination. The gradual decrease of this broad massif agreed with a progressive elimination of the surfactant, which was complete within only 50 min (see degradation kinetic curve in **Fig. S2**). Similar photodegradation kinetics was obtained with a solid film containing only P123, leaving a non-covered substrate after the process (see **Fig. S3**). While FTIR analysis is suitable to estimate the decomposition of P123, it does not take into account the removal of other organic compounds (devoid of CH bonds) which may be created during photocalcination and trapped into the material.

Note that no copolymer degradation occurred during the intermediate consolidation stage as assessed by FTIR spectroscopy (data not shown).

Table 3 illustrates the evolution of the siloxane microstructure (^{29}Si solid-state NMR data) after each of the three preparation steps. Clearly, the thermal consolidation resulted in a slight increase of the condensation degree (+ 8 %). While this value may appear low, skipping over this second step leads to a substantial loss of ordering. The formation of a short-range ordered mesostructure was indeed attested by XRD analysis (trace **d**, **Figure 3**), which revealed only a single low intense broad signal in low angles region. In the TEM images of this sample (insert of Figure 3) the parallel channels of the 2D hexagonal mesostructure were barely visible, suggesting a collapse of the silica walls. Accordingly, N_2 adsorption measurements resulted in a weak specific surface area ($41 \text{ m}^2 \text{ g}^{-1}$), indicative of a mostly dense sample. The main hypothesis for the loss of mesostructuration is an insufficient silica network condensation. Indeed, during thermocalcination, the silica network is also post-condensed by the temperature ramp inside the oven, ensuring a strong enough structure to withstand the concomitant surfactant removal. We can thus conclude that an intermediate post-condensation step between the two radiation steps is necessary. In addition, the first UV_B -driven mesostructuration step was found to be necessary. Although the low-pressure Hg arc serving in the last calcination step has an emission line at 254 nm matching the absorption range of the photoacid generator, a single-step UV_C irradiation ($t = 90 \text{ min}$) yielded a brittle delaminated film. P123 was only partially eliminated (10 %) and XRD analysis (trace **e**, Figure 3) revealed no mesostructuration. Consequently, each step has a specific role and cannot be removed.

3.2 Comparison between photo- and thermocalcination

Photocalcined and thermocalcined samples were compared as regards mesophase geometry, specific surface area and pore structural characteristics (size, size distribution and pore volume). Regarding the morphology, a strong analogy can be drawn between the two sample specimens as

revealed by TEM (**Figure 4**). In both cases, there was a conservation of the 2D hexagonal mesostructure with a preferential orientation of the mesostructure parallel to the substrate. In the photocalcined film, the entrance of the channels was visible in some areas exhibiting a well-defined honeycomb shape. From TEM images, pore widths were found to be equivalent after photocalcination (42 Å) and thermocalcination (41 Å). N₂ adsorption/desorption data in **Figure 5** revealed a type IV isotherm representative of mesoporous materials regardless of the calcination method. The photocalcined sample (**Figure 5A**) exhibited a triangular shape hysteresis, which may result from mesopores with narrow mouths (ink bottle pores) [29]. **Table 4** reports the specific surface area, pore volume (total and microporous) and pore widths calculated from BJH method (applied on the desorption branch) and TEM measurements. The photocalcined sample exhibited 224 m² g⁻¹ BET specific surface area, including 101 m² g⁻¹ due to microporosity. In contrast, the thermocalcined sample was devoid of micropores (BET specific surface area: 191 m² g⁻¹). It is hypothesized that photocalcination may allow a softer surfactant degradation, imposing less constraints on the fragile micropores. However, whether thermo- or photocalcined, the values of BET specific surface areas of our silica films can be regarded as moderate or low. Different reasons can be put forward to explain this result. Firstly, the micropore volume created by PEO segment/silica interactions may be minimized due to a limited solubility between PDMOS precursor (non-hydrolyzed oligomeric precursor) and PEO chains. Another hypothesis may be the strong vertical contraction of the film, which may shrink mesopores and eliminate the micropores on the silica walls through densification. Finally, because film thicknesses is relatively important compared to other mesoporous silica thin films (1000 – 2000 nm), there is the risk of structural non-homogeneities due to composition gradients created during drying, and possibly leading to poorly porous areas. Although the average pore size was the same for both thermo- and photocalcined films (~ 40 Å), the pore size distribution was slightly narrower in the photocalcined material (**Figure 5B**).

In order to examine the interest of photocalcination in terms of energy saving, the power consumption of a complete synthesis protocol including either photocalcination or thermocalcination

as final stage was evaluated (see details in **Table S1** in Data in Brief article). In the first case, the three-step process “UV_B-Δθ-Photocalcination” led to an estimated power usage of 0.36 kW h⁻¹, the final photocalcination step (0.25 kW h⁻¹) being the main contributor. In the second case, the two-step process “UV_B-thermocalcination” resulted in a power usage of 1.09 kW h⁻¹ using a conventional oven for calcination. Therefore, energy consumption could be reduced on average three-fold with a photocalcination, with a process twice as fast (128 min vs 270 min). Obviously, the “UV_B-thermocalcination” process could be improved by using a specific low-power muffle furnace (0.09 kW h⁻¹). Although the second protocol becomes now more energy-efficient, the “all UV method” remains a faster process.

3.3 Photocalcination kinetics: influence of experimental parameters

Irradiance. **Figure 6A** shows the plot of P123 degradation (FTIR data) as a function of UV_C irradiation time for the hybrid copolymer/silica sample (4 μm) prepared with 45 wt% P123. Photocalcination kinetics was similar at 63 and 50 mW cm⁻², and 50 min were necessary for a complete copolymer’s elimination. The degradation kinetics became gradually slower at 33 and 12 mW cm⁻², and consistently, longer irradiation times were required for the full removal of the surfactant. These results support the concept of a threshold irradiance value below which photodegradation rate start decreasing. In all instances, XRD patterns (**Fig. S4**) supported a conservation of the mesostructure without significant differences and the formation of a highly ordered mesostructure.

Surfactant concentration. **Figure 6B** depicts the same conversion vs time plots for hybrid mesostructured films (4 μm) containing 25, 45, 55 and 70 wt% P123 at two different irradiances (63 and 12 mW cm⁻²). Interestingly, elimination rate was not strongly dependent on the surfactant concentration, but much more influenced by the irradiance value as seen previously. At high UV_C irradiance (63 mW cm⁻²), an almost complete conversion was achieved after 50 min at 25 wt% P123

whereas it reaches 90 % at 70 wt% P123 after the same period. At lower irradiance (12 mW cm^{-2}), there was still a slight discrepancy between the kinetic profiles of the samples with again a fastest elimination at 25 wt% P123. In addition, one must note substantial differences in terms of mesostructure between the samples (see XRD patterns in Fig. S5): at 25 wt% P123, poorly organized samples were produced; in the 35-55 wt% range, highly ordered 2D hexagonal structure; and at 70 wt%, the sample was lamellar. The corollary is that not only P123 concentration but also mesophase geometry/ordering have a restricted impact on photocalcination progress.

Film thickness. Figure 6C shows the effect of film thickness ($0.2 - 4 \mu\text{m}$) on photocalcination kinetics ($I = 63 \text{ mW cm}^{-2}$). Clearly, photocalcination was faster upon decreasing film thickness for a hybrid sample prepared with 45 wt% P123. Conversion rate was almost doubled at $0.2 \mu\text{m}$ compared to $4 \mu\text{m}$, implying a photocalcination time reduced to 30 min instead of 50 min. In most cases, the XRD patterns were consistent with a mesostructure preservation after photocalcination (Fig. S6).

3.4 Photocalcination mechanism

With an irradiation at 165 and 254 nm, photocalcination mechanism may rely on *photoablation* and/or *photooxidation*.

- Polymer photoablation has been extensively described with excimer lasers (mostly at 193 nm and 248 nm) [30, 31] and requires generally a strong absorption of the polymer materials, which is usually the case in the UV_C range. However, polyethers such as PEO or PPO have a relatively restricted absorption range below 190-220 nm [32]. Consequently, P123 is expected to absorb only the 185 nm line. In photoablation, electronic excitation after radiation absorption at 185 nm may cause a direct chemical bond cleavage (C-H, C-O, C-C) (photochemical effect), or the electronic excited states can lose their energy by a series of non-radiative transitions that result in a general heating of the material (photothermal effect). Possibly, both thermal and photochemical effects may operate simultaneously [33].

- In the second degradation mechanism, the material can be altered by photooxidation through the action of ROS: mainly ozone O_3 , hydroxyl radicals OH^\bullet and singlet oxygen 1O_2 . The photochemical generation of these species has been extensively described [34]. At 185 nm, ozone can be produced from triplet ground state oxygen 3O_2 . 1O_2 can be generated by photolysis of ozone at 254 nm, while OH^\bullet is the main product from the reaction of 1O_2 with water. Despite previous studies on photocalcination (Table 1), the question of the mechanism is still an ongoing discussion. In our system, two experiments were performed to elucidate the P123 photocalcination mechanism using systematically a P123/silica sample having a copolymer concentration of 45 wt%.

Effect of emission line: with our low-pressure amalgam arc made of synthetic quartz envelope, two lines at 185 nm and 254 nm are emitted. Changing to conventional quartz enabled to absorb the 185 nm line, resulting in a single emission line at 254 nm. **Figure 7A** shows the difference of conversion rates between the two lamps keeping the overall UV_C irradiance constant at 44 mW cm^{-2} ($I_{254} = 33 \text{ mW cm}^{-2} / I_{185} = 11 \text{ mW cm}^{-2}$ in the dual emission, and $I_{254} = 44 \text{ mW cm}^{-2}$ for the single emission). It is clear that the 185 / 254 nm dual emission induced much faster kinetics: after 50 minutes, 5 times more surfactant was eliminated. Consequently, the 185 nm line seems to be mainly responsible for the degradation process. Because the 185 nm line can be involved either in photooxidation and photoablation, it is not possible at this stage to outline a specific degradation pathway.

Effect of atmosphere: an additional photocalcination experiment was thus performed in a closed system purged and continuously fed by argon, eliminating the possibility to produce ROS. Degradation kinetics in **Figure 7B** indicated that photocalcination was poorly affected by the atmosphere's composition. There was only a 5 % increase of conversion after 30 min when the reaction was performed in air compared to argon. Therefore, the hypothesis of having ROS-driven oxidation as the main degradation reaction can be set aside, and photoablation can be advanced as the main pathway contributing to photocalcination. Nevertheless, the role of photooxidation cannot be entirely minimized as evidenced by the short acceleration in presence of oxygen (**Figure 7B**) and

the slow degradation occurring at 254 nm only (**Figure 7A**). These two cases demonstrate the complementary, although minor, role played by the ROS.

The main photodegradation mechanism based on photoablation is controversial, and has been established in the literature only for a limited number of polymers such as poly(methyl methacrylate) [35]. In our case, the decomposition reactions, the ratio between the two photochemical and photothermal mechanisms, the degradation products (all highly dependent on irradiation wavelength and the polymer) need to be clarified. All these aspects have not been investigated with Pluronic (poloxamer) or even polyethers.

Conclusion

Coupling photoinduced mesostructuration and calcination has resulted in a unique “all UV methodology” to mesoporous silica thin films. Starting from a 4 μm thick film containing 45 wt% P123, a mesostructured copolymer/silica hybrid film was first produced within 30 min (UV_B irradiation, fluorescent tube), then 50 additional min (UV_C , low-pressure amalgam arc) were necessary for a complete removal of the templating agent. Essential to keep mesostructure’s integrity has been a short (8 min) intermediate thermal consolidation of the siloxane network at 150 $^{\circ}\text{C}$ between these two photochemical treatments. Compared with a route involving thermocalcination, energy consumption has been reduced on average three-fold and synthesis times have been twice as fast (128 min vs 270 min). Whatever the method, both mesostructure and siloxane degree of condensation were similar. However, photocalcination has led to a higher specific surface area ($224 \text{ m}^2 \text{ g}^{-1}$) through a better conservation of microporosity. Surfactant elimination rate has been strongly accelerated upon decreasing film thickness but hardly affected by copolymer concentration. Clearly, the high output power provided by this low-pressure indium-mercury amalgam arc is a determining factor for the fast photocalcination kinetics. With regard to

photocalcination mechanism, the 185 nm line has the lead role and drives a photoablation effect together with secondary photooxidation reactions.

Acknowledgements

This work was supported by the Fondation de l'École Nationale Supérieure de Chimie de Mulhouse (France) which has granted a 3-year PhD scholarship to Mrs. Mathilde Sibeaud. We acknowledge the adsorption technical platform of Institut de Sciences des Matériaux de Mulhouse for performing N₂ adsorption and desorption isotherms.

References

- [1] D. Zhao, Y. Wan, W. Zhou, Applications of Mesoporous Molecular Sieves, Ordered Mesoporous Materials, Wiley-VCH, 2013, pp. 465-511.
- [2] A. Stein, B.J. Melde, R.C. Schroden, Adv. Mater., 12 (2000) 1403-1419.
- [3] M.E. Davis, Nature, 417 (2002) 813-821.
- [4] P. Innocenzi, L. Malfatti, Chem. Soc. Rev., 42 (2013) 4198-4216.
- [5] C. Sanchez, P. Belleville, M. Popall, L. Nicole, Chem. Soc. Rev., 40 (2011) 696-753.
- [6] M. Sibeaud, H. De Paz-Simon, C. Croutxé-Barghorn, S. Rigolet, L. Michelin, B. Lebeau, L. Vidal, P.A. Albouy, A. Chemtob, Microporous Mesoporous Mater., 257 (2018) 42-50.
- [7] F. Bérubé, S. Kaliaguine, Microporous Mesoporous Mater., 115 (2008) 469-479.
- [8] F. Kleitz, W. Schmidt, F. Schüth, Microporous Mesoporous Mater., 65 (2003) 1-29.
- [9] Y. Chua, C.X.C. Lin, F. Kleitz, S. Smart, Desalination, 370 (2015) 53-62.
- [10] S.S. Park, B. An, C.S. Ha, Microporous Mesoporous Mater., 111 (2008) 367-378.
- [11] N. Ehlert, P.P. Mueller, M. Stieve, T. Lenarz, P. Behrens, Chem. Soc. Rev., 42 (2013) 3847-3861.
- [12] T. Sharma, Y. Hu, M. Stoller, M. Feldman, R.S. Ruoff, M. Ferrari, X.J. Zhang, Lab Chip, 11 (2011) 2460-2465.

- [13] G. Wirnsberger, B.J. Scott, G.D. Stucky, *Chem. Commun.*, (2001) 119-120.
- [14] S.G. de Avila, L.C.C. Silva, J.R. Matos, *Microporous Mesoporous Mater.*, 234 (2016) 277-286.
- [15] V. Cauda, C. Argyo, D.G. Piercey, T. Bein, *J. Am. Chem. Soc.*, 133 (2011) 6484-6486.
- [16] L. Xiao, J. Li, H. Jin, R. Xu, *Microporous Mesoporous Mater.*, 96 (2006) 413-418.
- [17] L.M. Yang, Y.J. Wang, G.S. Luo, Y.Y. Dai, *Microporous Mesoporous Mater.*, 81 (2005) 107-114.
- [18] T. Clark, J.D. Ruiz, H. Fan, C.J. Brinker, B.I. Swanson, A.N. Parikh, *Chem. Mater.*, 12 (2000) 3879-3884.
- [19] A. Hozumi, H. Sugimura, K. Hiraku, T. Kameyama, O. Takai, *Chem. Mater.*, 12 (2000) 3842-3847.
- [20] A.M. Dattelbaum, M.L. Amweg, J.D. Ruiz, L.E. Ecke, A.P. Shreve, A.N. Parikh, *J. Phys. Chem. B.*, 109 (2005) 14551-14556.
- [21] U.H. Lee, Y.K. Hwang, Y.U. Kwon, Mesoporous titania thin film with cubic mesostructure using photocalcination, in: S.E. Park, R. Ryoo, W.S. Ahn, C.W. Lee, J.S. Chang (Eds.) *Nanotechnology in Mesostructured Materials 2003*, pp. 77-80.
- [22] H. De Paz-Simon, A. Chemtob, C. Croutxé-Barghorn, S. Rigolet, L. Michelin, L. Vidal, B. Lebeau, *APL Mater.*, 2 (2014) 113306.
- [23] A.M. Dattelbaum, M.L. Amweg, L.E. Ecke, C.K. Yee, A.P. Shreve, A.N. Parikh, *Nano Lett.*, 3 (2003) 719-722.
- [24] B. Eliasson, U. Kogelschatz, *Ozone: Sci. Eng.*, 13 (1991) 365-373.
- [25] A. Keogh, C. Thompson, B.J. Phillips, Kitchen exhaust ultraviolet system, WO 2009092546A3, 2010.
- [26] W. J.Kowalski, *Ultraviolet Germicidal Irradiation Handbook: UVGI for Air and Surface Disinfection*. Springer, Heidelberg, Germany, 2009.
- [27] J. R. Bolton, C.A. Cotton, *The Ultraviolet Disinfection Handbook*, 1st ed. American Water Works Association, Denver, USA, 2008.
- [28] D. Massiot, F. Fayon, M. Capron, I. King, S. Le Calvé, B. Alonso, J.-O. Durand, B. Bujoli, Z. Gan, G. Hoatson, *Magn. Reson. Chem.*, 40 (2002) 70-76.

- [29] D. Zhao, Y. Wan, W. Zhou, Structural Characterization Methods, Ordered Mesoporous Materials, Wiley-VCH Verlag, 2013, pp. 117-151.
- [30] R. Srinivasan, V. Mayne-Banton, Appl. Phys. Lett., 41 (1982) 576-578.
- [31] Y. Kawamura, K. Toyoda, S. Namba, Appl. Phys. Lett., 40 (1982) 374-375.
- [32] J.F. Rabek, Polymer Photodegradation: Mechanisms and experimental methods, Chapman Hall, London (UK), 1994.
- [33] S.G. Hansen, T.E. Robitaille, J. Appl. Phys., 62 (1987) 1394-1399.
- [34] J.R. Vig, J. Vac. Sci. Technol., 3 (1985) 1027-1034.
- [35] L. Urech, T. Lippert, Photoablation of Polymer Materials, in: Photochemistry and Photophysics of Polymer Materials, John Wiley & Sons, (2010) 541–568.

Table 1: Main studies on photocalcination for the preparation of mesoporous films.

References	[18]	[19]	[20]	[21]	[22]	[23]
Film thickness	100 nm	200 nm	~100 nm	n/a	7 μm	n/a
Templating agent	Brij 56	CTAB or CTAC	Brij 56	Brij type	P123	Brij 56
Irradiation source	185 / 254 nm. Low-pressure Hg arc	172 nm. Xe ₂ * excimer lamp	185 / 254 nm. Low-pressure Hg arc	Low-pressure Hg arc	254 – 800 nm medium-pressure Hg arc	185 / 254 nm low-pressure Hg arc
Irradiance	n/a	10 mW cm ⁻²	n/a	n/a	400 mW cm ⁻²	n/a
Photocalcination duration	60 to 120 min	30 min (10 ⁵ Pa) 3h (10 Pa)	90 min	45 min	190 min	180 min

Table 2: Irradiance values as a function of the lamp-sample distance

Lamp-sample distance	1.5 cm	3 cm	6 cm	12 cm
Total estimated irradiance in UV _c (mW cm ⁻²)	60	44	29	10
Estimated irradiance at 185 nm (mW cm ⁻²)	19	11	7	1
Estimated irradiance at 254 nm (mW cm ⁻²)	41	33	21	9

Table 3: condensation degree of the siloxane network obtained from ²⁹Si MAS+DEC spectra of PDMOS/P123 sample ([P123] = 45 wt% with respect to PDMOS) during the different preparation steps. Q₀ and Q₁ species are not observed.

Synthesis step	Q ₂	Q ₃	Q ₄	Condensation degree ($\pm 5\%$)
Step a Photoinduced mesostructuration	15	60	25	78
Step b. Thermal consolidation	3	47	50	86
Step c. Photocalcination	3	35	62	90
Step c'. After direct thermocalcination	5	32	63	89

Table 4: Specific surface area, pore volumes and pore widths obtained from the N₂ adsorption experiments and TEM analysis for silica films prepared with a P123 concentration of 45 wt%.

Synthesis method	Synthesis involving Photocalcination	Synthesis involving Thermocalcination
BET specific surface area ^a (m ² g ⁻¹)	224	191
Total pore volume ^a (cm ³ g ⁻¹)	0.17	0.30
t-Plot micropore volume ^a (cm ³ g ⁻¹)	0.04	-
BJH desorption pore width ^a (Å)	40	39
Pore width ^b (Å)	42	41

^a determined by N₂ adsorption measurements, ^b determined by TEM data

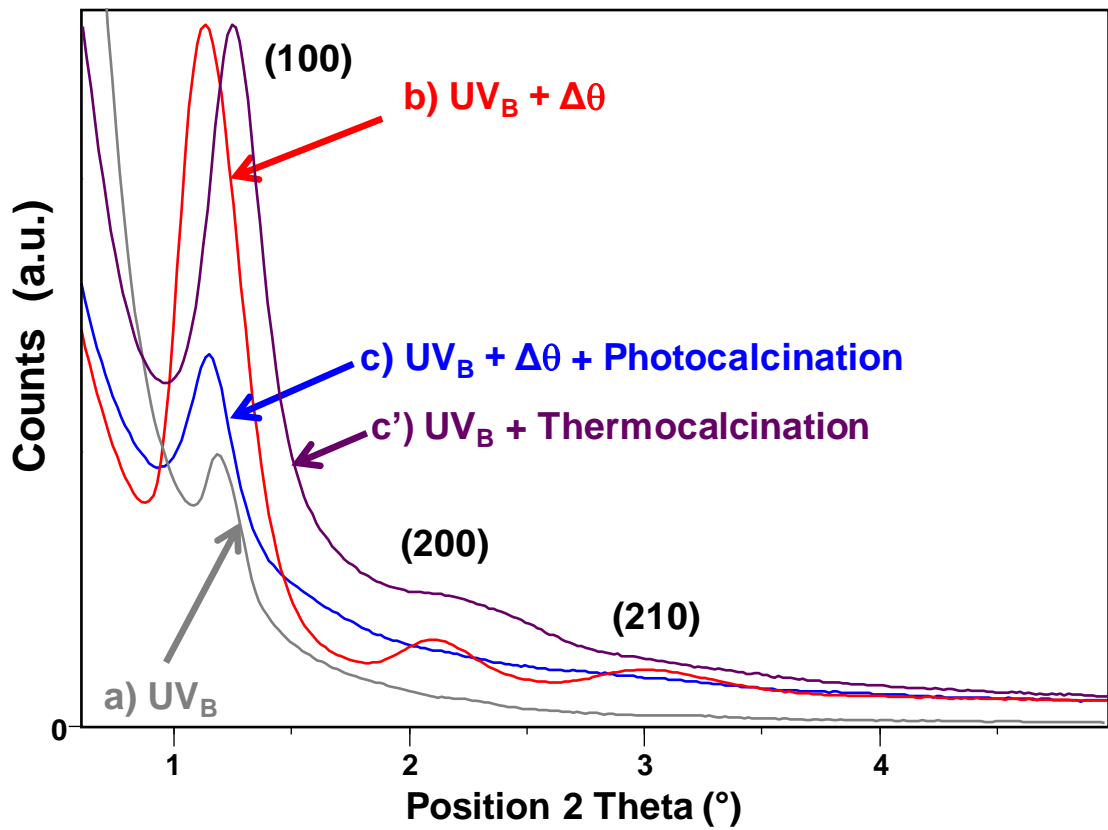


Figure 1: XRD patterns of P123/silica film containing 45 wt% P123 after three consecutive synthetic steps: a) UV_B irradiation (photoinduced mesostructuration); b) thermal post-consolidation; and c) UV_C irradiation (photocalcination). In pattern c', the same film was subjected successively to UV_B irradiation and thermocalcination.

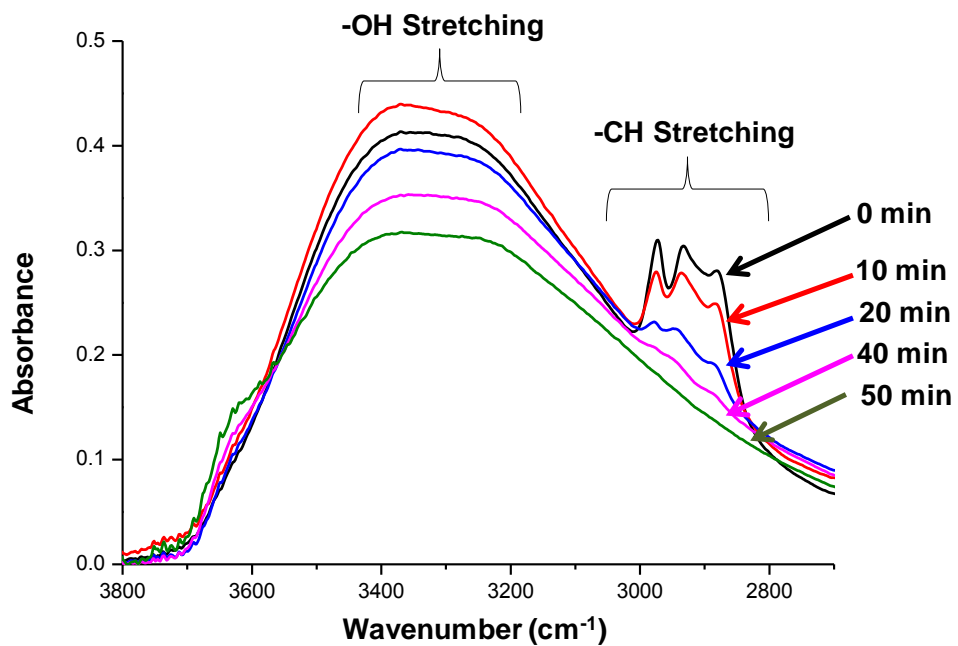


Figure 2: FTIR spectra of 45 % P123/Silica film under UVC irradiation (photocalcination) for various irradiation times in the 2800 -3800 cm⁻¹ range. Photocalcination was performed until the -CH stretching bands of P123 were no longer visible.

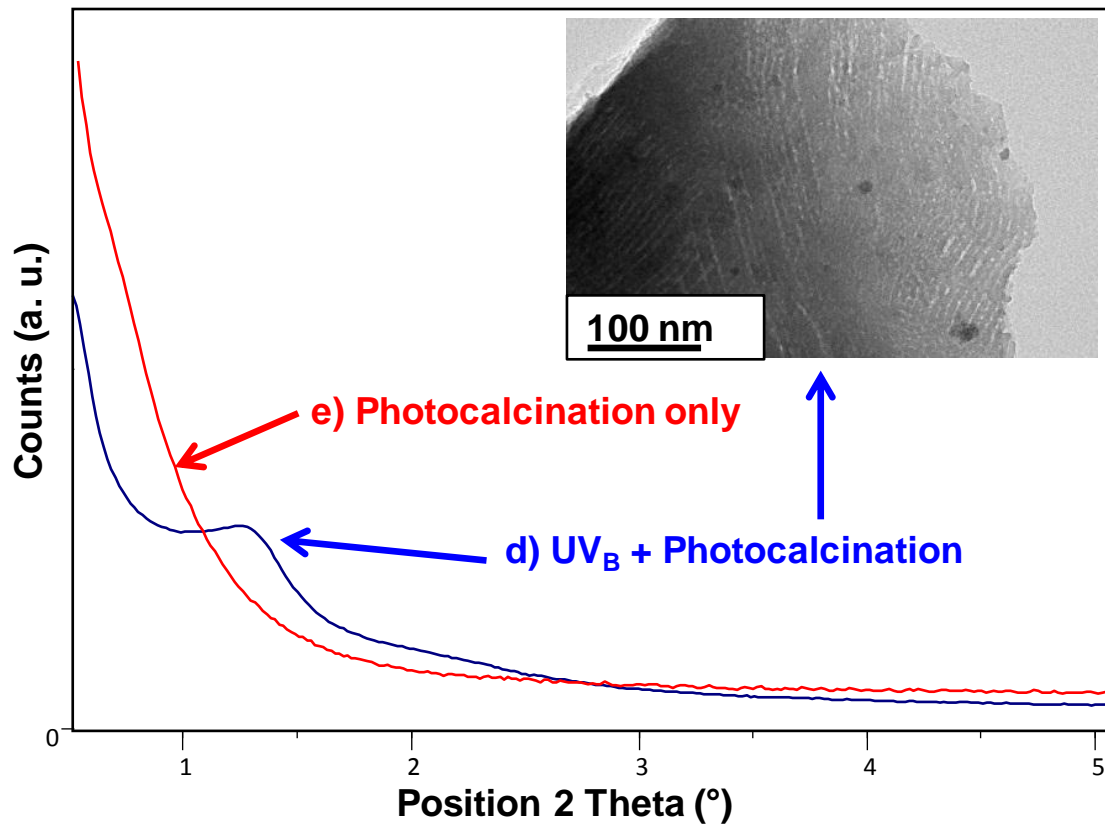


Figure 3: XRD patterns of a PDMS/P123 films containing 45 wt% P123 obtained after two successive UV_B irradiation and UV_C irradiation without thermal treatment (trace **d**). Insert: TEM image of a mesoporous silica sample after direct photocalcination. Using only UV_C irradiation resulted in a featureless pattern indicative of an amorphous structure (trace **e**).

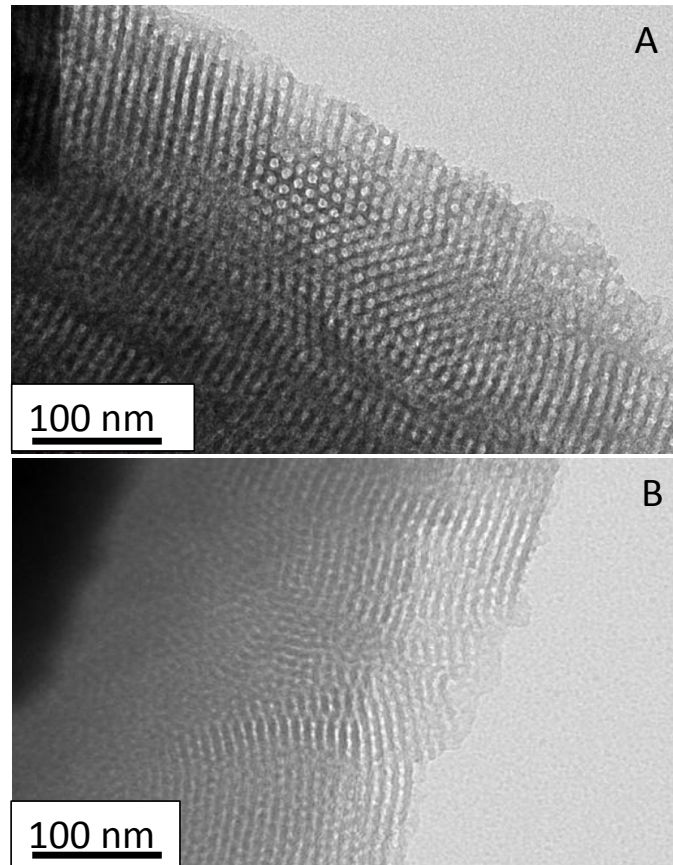


Figure 4: TEM images of mesoporous silica films prepared with 45 wt% P123 via two different methodologies: A) $UV_B + \Delta\theta$ + Photocalcination, and B) UV_B + Thermocalcination.

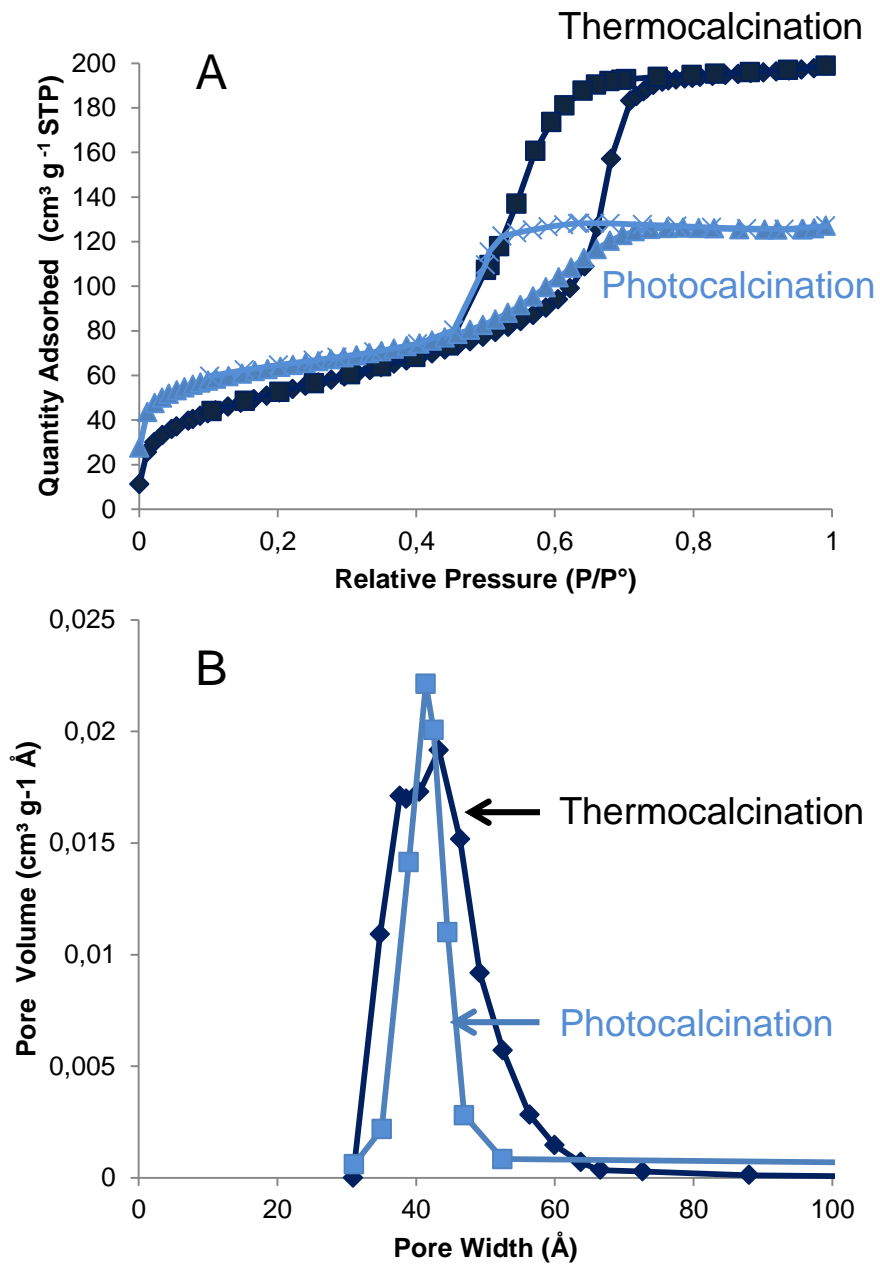


Figure 5: N_2 adsorption/desorption isotherms (**A**) and BJH pore size distribution (**B**) determined from desorption branches for mesoporous silica films prepared with 45 wt% P123 via two different methodologies: 1) $\text{UV}_B + \Delta\theta + \text{Photocalcination}$, and 2) $\text{UV}_B + \text{Thermocalcination}$.

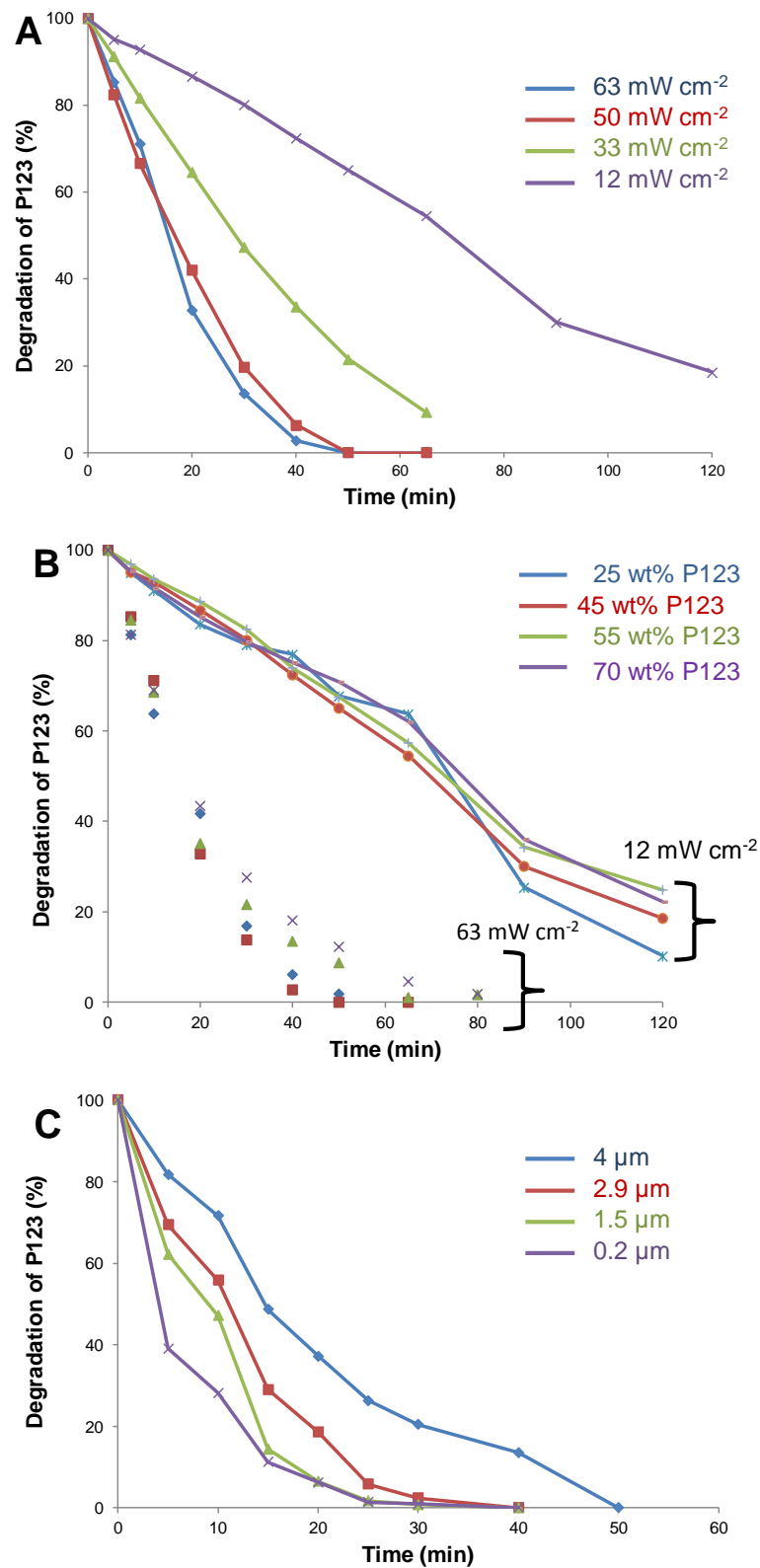


Figure 6: Effect of irradiance (A), P123 content (B), and film thickness (C) on photocalcination kinetics. Films were prepared following a three-step methodology: UV_B + Δθ + Photocalcination. When not mentioned, the P123/silica film has a film thickness of 4 μm, a concentration of P123 of 45 wt% and UV_C irradiance to carry out photocalcination was 63 mW cm⁻².

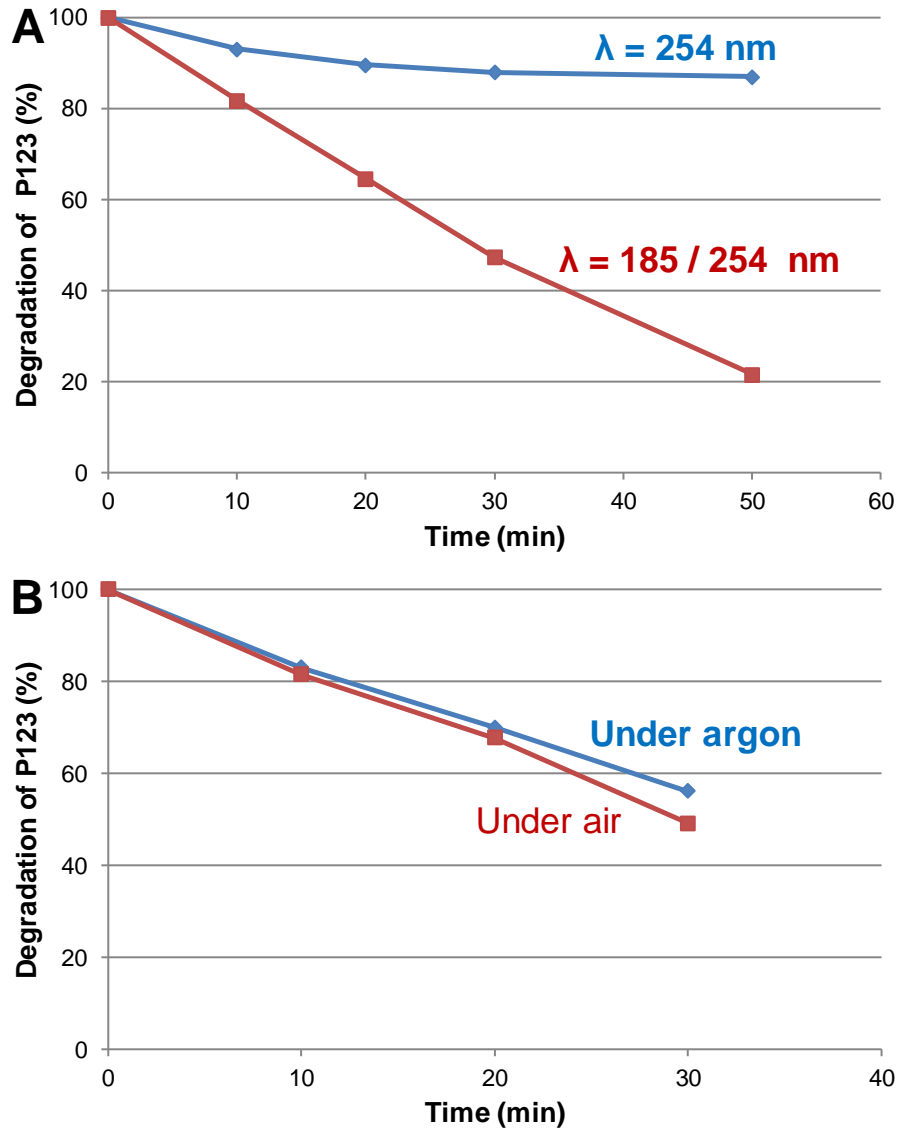


Figure 7: Effect of radiation wavelength (**A**) and atmosphere composition (**B**) on photocalcination kinetics of 45 wt% P123/silica film. In plot **A**, the overall UV_c irradiance is similar (44 mW cm⁻²).